

# Including Atmospheric Extinction in a Performance Evaluation of a Fixed Grid of Solar Panels

Kevin Krisciunas<sup>1,2</sup>

## ABSTRACT

We characterize the performance of a fixed grid of solar panels on the basis of data taken under clear sky conditions over 12 months. We confirm that the power output is linearly proportional to  $\cos(\theta)$ , where  $\theta$  is the angular difference of direction toward the Sun and the vector perpendicular to the panels. In order to confirm this we applied methods from astronomical photometry reduction. From late March through August we find that the median effective atmospheric extinction term is 0.145 mag/airmass. From October to mid-March the median extinction term is 0.081 mag/airmass. The proportionality “constant” scaling  $\cos(\theta)$  appears to be seasonally dependent, with the smallest scaling factors occurring when the extinction term is largest. Finally, we find that extinction-corrected power often underperforms the linear relationship late in the morning or early in the afternoon. This is most likely because the efficiency of solar panels depends on their operating temperature, and the panel temperature increases over the course of time on a sunny day.

*Subject headings:* photometry - techniques

## 1. Introduction

On 26 April 2021 Texas Green Energy installed two sets of solar panels on my house in College Station, Texas (latitude N 30° 33′ 43″, longitude W 96° 16′ 8″, elevation 85 m).<sup>3</sup> Six

---

<sup>1</sup>Texas A. & M. University, Department of Physics & Astronomy, 4242 TAMU, College Station, TX 77843; krisciunas@physics.tamu.edu

<sup>2</sup>George P. and Cynthia Woods Mitchell Institute for Fundamental Physics & Astronomy

<sup>3</sup>Engineered in Germany by Q.CELLS, the panel model is Q.PEAK DUO BLK-G6+ 330-345. Basic information on photovoltaic cells can be found here: <https://www.energy.gov/eere/solar/articles/pv-cells-101-primer-solar-photovoltaic-cell>. Also useful is this website: <https://sciencing.com/effect-wavelength-photovoltaic-cells-6957.html>

panels are mounted on the upper roof, and seven panels on the lower roof (Fig. 1). After engineers, technicians, and city inspectors were done with their work, the system went live on 8 June. Over the course of one year the system has generated 6516 kilowatt-hours (kWh) of power, or an average of 18 kWh per day.

Solar panels produce electric power by means of the photovoltaic effect. The photoelectric effect, on the other hand, involves the ejection of electrons from a conducting plate when light shines on it. However, the photovoltaic effect takes place at the boundary of two semiconducting plates. Electrons are not ejected. They accumulate along the boundary of the semiconducting plates and create a voltage. When the plates are connected with a wire, a current flows in the wire.

Our solar panels contain crystalline silicon as the semiconducting material. One key parameter is the “band gap energy” of crystalline silicon. Only photons with energy greater 1.11 electron volts can dislodge electrons from silicon atoms and send them into the conduction band between the two semiconducting plates. The longest wavelength light usable by the solar panels is near-infrared light at a wavelength of 1.1 microns. Much shorter wavelength photons, with energy greater than 3 eV, send electrons out of the conduction band, rendering them unable to do work. The corresponding wavelength is about 413 nanometers (corresponding to violet light). Thus, solar panels that use silicon as the semiconducting material convert sunlight with wavelengths ranging from 0.413 to 1.1 microns into electric power. The author does not know of a “response curve” of solar panels as a function of wavelength, but the mean wavelength of sensitivity is about 760 nm. This is between the effective wavelengths of the photometric *R*- and *I*-bands at 650 and 800 nm, respectively (or the corresponding Sloan *r*- and *i*-bands).

According to the installers, our panels face azimuth  $135^\circ$  (i.e., southeast). The pitch of the upper set of panels was measured by them to be  $24^\circ$ . Later we did our own measurements using a phone application called Measure and found that the upper set of panels is pitched  $23.3^\circ$  to the horizontal, while the lower set of panels is pitched  $20.2^\circ$  to the horizontal. We adopt the average value ( $21.75^\circ$ ) for subsequent analysis.

The vector perpendicular to the panels intersects the celestial sphere at azimuth  $135^\circ$  and elevation angle  $68.25^\circ$  in the horizon system of celestial coordinates.<sup>4</sup> Let us call this position P. Its elevation angle and azimuth has an uncertainty of perhaps  $\pm 1$  deg in each coordinate. Such uncertainty will not have a significant effect on the main results presented here.

---

<sup>4</sup>Basic information on the celestial sphere can be found online at [http://people.tamu.edu/~kevinkrisciunas/cel\\_sphere.html](http://people.tamu.edu/~kevinkrisciunas/cel_sphere.html) .

Now, just as the sky is brighter and brighter during morning twilight, and the world outside is not pitch dark on a cloudy day, solar panels can generate some power even if no sunlight is directly incident upon them. However, since light from the Sun’s photosphere is so much brighter than sunlight scattered by the various components of the Earth’s atmosphere, here we try to characterize the power output from the solar panels solely from direct sunlight. To characterize the performance of the solar panels we will need to calculate the elevation angle and azimuth of the Sun at multiple times on any given day.

For an object like the Sun that transits the celestial meridian south of the zenith for an observer in the northern hemisphere situated north of the Tropic of Cancer,<sup>5</sup> the maximum elevation angle above the horizon will be:

$$h_{max} = [90^\circ - \phi] + \delta_\odot, \quad (1)$$

where  $\phi$  is the latitude of the observer and  $\delta_\odot$  is the declination of the Sun. Over the course of the year  $h_{max}$  has a range of  $47^\circ$  (twice the tilt of the Earth’s axis of rotation to the plane of its orbit).

Let  $\theta$  be the angular distance between position P mentioned above and the position of the Sun on the celestial sphere. Of course, due to the rotation of the Earth, the elevation angle and azimuth of the Sun change continuously, so  $\theta$  changes continuously.

Fig. 2 is a plot of raw data obtained from 9 June to 21 August 2021 and tabulated in Table 1. The reader will notice that the data are not symmetric. Starting about 15:15 CDT a summer day, the lower panels are more and more in shadow. We will not consider any further those measurements in Table 1 taken after 15:15 local time. Also, one should note that the data obtained from 7 to 10 AM Central Daylight Time show very little scatter from day to day. By noontime something else is happening. We believe it is related to the efficiency of the solar panels as a function of operating temperature (see Discussion below).

Table 2 contains raw data from three particular days that will be discussed below. Raw data for 17 other days analyzed in this paper can be obtained from the author by request.

In Fig. 3 we plot one year’s worth of raw data in a 3D projection plot. A few data points were excluded: those taken when there was frost on the solar panels, and those taken when some of the panels were in shadow. Altogether, 333 data points are plotted.

According to the specifications on solar panels, their output varies proportionally to

---

<sup>5</sup>In Hilo, Hawaii, for example, at latitude  $+19.7^\circ$ , the Sun transits the celestial meridian *north* of the zenith for about two months each year starting on May 18th.

$\cos(\theta)$ . This can be demonstrated by having a set of solar panels that can track the Sun, compensating for the rotation of the Earth. The user would also want to be able to aim the panels any number of degrees to the right or left, and above or below the direction to the Sun. This is beyond the capabilities of our system. That is just as well, as the local Home Owners Association would veto a plan to install such a system.

We will be able to demonstrate the cosine law. But first we must discuss some basics of astronomical photometry.

## 2. Astronomical Photometry

In this section we present an example that shows, in effect, if you observe an astronomical source and plot the logarithm of the number of photons per second detected vs. a measure of the path length through the Earth’s atmosphere, you can fit the data with a straight line. The slope of that line is called the atmospheric extinction coefficient.

Astronomical photometry dates back to the time of Hipparchus (ca. 150 B.C.), who classified the brightness of the stars using magnitude bins. The brightest stars in the sky were defined to be magnitude 1 (i.e., stars of the first class), while the faintest stars visible to the unaided eye are magnitude five or six. Using a nineteenth century formulation of magnitudes, a first magnitude star gives us exactly 100 times as many photons per second as a sixth magnitude star. In the nineteenth century Karl August Steinheil and Gustav Theodor Fechner demonstrated that the impression we have of the brightness of a light source is proportional to the logarithm of the light intensity. This relationship holds for hearing and for taste and is known as the Weber-Fechner psychophysical law (Herrmann 1984, pp. 70-76).

If we measure  $f_1$  photons per second from a bright star and  $f_2$  from a second (fainter) star, then by definition the *difference* of their apparent magnitudes is  $-2.5 \log_{10} (f_1/f_2) = \Delta m$ . Since  $f_1/f_2 > 1.0$ ,  $\Delta m$  is negative. Similarly,  $a^{\Delta m} = f_1/f_2$ , where  $a$  is equal to the fifth root of 100, or approximately 2.51186.

Consider a schematic diagram of a plane parallel atmosphere (Fig. 4). A star at zenith angle  $z$  is observed through a longer path length of atmosphere than it would be at the zenith. (The zenith angle is  $90^\circ$  minus the elevation angle.) For  $z < 60^\circ$  that path length, divided by the path length towards the zenith, is simply  $\sec(z)$ . We call the ratio of these path lengths the “air mass” ( $X$ ), which is a unitless parameter. It is *not* a column density of molecules and atoms measured through the atmosphere. For  $z < 60^\circ$ ,  $X = \sec(z)$  is a good approximation. This is calculated using spherical trigonometry.

For zenith angles greater than  $60^\circ$  (i.e., air mass greater than 2.0) the plane parallel approximation of the atmosphere breaks down. After all, the atmosphere is essentially a large number of thin spherical shells whose density decreases with altitude. Also, for objects viewed near the horizon we have to consider atmospheric refraction. These considerations are beyond the scope of the present paper. For our purposes here we may use the following formula from Hardie (1962):

$$X = \sec z - 0.0018167 (\sec z - 1) - 0.002875 (\sec z - 1)^2 - 0.0008083 (\sec z - 1)^3 . \quad (2)$$

We note that this formula breaks down for zenith angles greater than  $87^\circ$ .

Nowadays we take celestial images using a telescope and solid state cryogenically-cooled charge-coupled device (CCD), using a number of photometric filters, such as a blue filter called  $B$  and a yellow-green filter called  $V$ . These two filters have transmission curves that peak at about 440 and 550 nm, respectively. Instrumental magnitudes can be determined by displaying the images with SAO Image DS9 and doing aperture photometry in the IRAF environment.<sup>6</sup>

How does one reduce the data? Experts give conflicting advice. As my colleague George Wallerstein (1930-2021) used to say, “Four astronomers, five opinions.” For simplicity’s sake, using software like IRAF one designates the radius in pixels of an aperture, centers one star in the aperture, and determines the number of digital counts above the sky level. IRAF calculates  $\text{minus } 2.5 \log_{10}$  of those counts and adds  $2.5 \log_{10}$  of the integration time in seconds.<sup>7</sup> This gives an instrumental magnitude adjusted to an integration time of one second. From the telescope operating system the image file headers contain the air mass values.

Say one has taken  $B$ -band and  $V$ -band images of fields of standard stars, such as those of Landolt (1992, 2007). One ends up with instrumental  $b$  and  $v$  magnitudes. The simplest transformation of the instrumental  $v$  magnitudes and instrumental  $b - v$  colors to standardized  $V$ -band values in the photometric system of Landolt is:

---

<sup>6</sup>IRAF is distributed by the National Optical Astronomy Observatory, which is operated by the Association of Universities for Research in Astronomy, Inc., under cooperative agreement with the National Science Foundation (NSF).

<sup>7</sup>IRAF also adds an arbitrary constant here, defaulted to 25. This is to give instrumental magnitudes that are positive and comparable to what the eventual reduced values become.

$$V = v - k_v X + CT_v(b - v) + \zeta_v, \quad (3)$$

where:  $k_v$  is the  $V$ -band atmospheric extinction coefficient;  $CT_v$  is a color term used to correct for differences of transmission as a function of wavelength of the filters used by the observer and the ones used by Landolt; and  $\zeta_v$  is a photometric zero point (or, simply, the  $Y$ -intercept of some regression line). If the stars range in color from very blue to very red and/or the observations were made over a wide range of air mass, one may have to add second order terms to Eq. 3.

Using IRAF or equivalent FORTRAN or PYTHON code, one can solve simultaneously for the extinction term, color term, and zero point. (We are effectively fitting the best plane to a three dimensional set of data.) If the color term is known robustly, then one can take the difference of the color-corrected instrumental  $v$  magnitudes and Landolt's standardized values and plot these magnitude differences vs. the air mass values to obtain the extinction term and the photometric zero point.

Fig. 5 shows an example of determining the atmospheric  $V$ -band extinction coefficient, using data taken by us with the 0.9-m telescope at Cerro Tololo Inter-American Observatory (CTIO) on 26 November 2005 (UT). We plot the color-corrected instrumental magnitudes ( $v + CT_v(b - v)$ ) minus the catalogue magnitudes ( $V$ ) vs. the air mass values. The slope gives the  $V$ -band extinction coefficient  $k_v$ .

If the sky is clear and has stable transparency, one can convert all of the raw measurements taken on a given night to standardized, publishable values, with random errors of  $\pm 0.02$  magnitudes or better (roughly 2 percent). In Fig. 5 we find a  $V$ -band extinction coefficient of  $0.164 \pm 0.005$  mag/airmass and a root-mean-square (RMS) residual of  $\pm 0.013$  mag, after eliminating one  $5\text{-}\sigma$  outlier from the regression. This may be compared to the median  $V$ -band extinction of 0.154 mag/airmass from 29 nights of observations by us at CTIO and Las Campanas Observatory (LCO) from 21 April 2001 through 21 December 2012. In our experience, under clear sky conditions the extinction values in a particular photometric band at a particular site can vary from night to night at least  $\pm 50$  percent compared to the mean or median value.

### 3. Demonstrating the Cosine Law

One records the power produced by the solar panel system (from a digital display) over a wide range of the Sun's elevation angle under clear sky conditions. One then proceeds to calculate the elevation angle and azimuth of the Sun for each observation time using the

right ascension and declination of the Sun. One can look up  $\alpha_{\odot}$  and  $\delta_{\odot}$  in the annual volume of the *Astronomical Almanac* and interpolate to local noontime for any given day. Or one can use the method of van Flandern & Pulkkinen (1979) to obtain  $\alpha_{\odot}$  and  $\delta_{\odot}$  to the nearest arc minute.<sup>8</sup>

Using a program written by us, one can set the date, latitude and longitude of the site, and the right ascension and declination of the Sun to calculate the Sun’s azimuth, elevation angle, and air mass for all the corresponding times of day. Then, one calculates the values of angle  $\theta$ , the angular distance between point P (azimuth  $135^{\circ}$ , elevation angle  $68.25^{\circ}$ ) and the azimuth and elevation angle of the Sun at the times in question. A plot of the measured power ( $P_{meas}$ ) vs.  $\cos(\theta)$  from 16 June 2021 is found in the top half of Fig. 6. It is encouraging that the data show a linear relation, but it is clear that a linear fit does not pass through the origin. It certainly should do so, because the panels begin generating significant power shortly after sunrise once the Sun’s light is incident on the panels.

We can correct the measured values of the power to the equivalent values we would have obtained if the Sun were at the zenith. Consider that the Sun observed at zenith angle  $z$  is dimmer than it would be at the zenith. (See Fig. 4.) To correct the observed power to what we would measure with the Sun at the zenith we must multiply the observed power by

$$10^{(0.4 \times \text{extinction term} \times \text{path length difference})} = 2.51186^{k_{\lambda}(X_{\odot} - 1)} .$$

The extinction term  $k_{\lambda}$  is the effective extinction in magnitudes per airmass integrated over the wavelength range at which the solar panels operate (0.4 to 1.1 microns).

Thus, the power we would measure with the solar panels if the Sun were at the zenith (airmass 1) is related to the power when the Sun’s airmass is  $X_{\odot}$  as follows:

$$P_{extcorr} = 2.51186^{k_{\lambda}(X_{\odot} - 1)} \times P_{meas} . \tag{4}$$

For the physicist or engineer who is confused or horrified by an encounter with the stellar magnitude system, a relation equivalent to Eq. 4 can be written as follows:

$$P_{extcorr} = e^{\alpha(X_{\odot} - 1)} \times P_{meas} , \tag{5}$$

where  $\alpha = 0.92103 k_{\lambda}$ .

---

<sup>8</sup>A table of the Sun’s coordinates for each day of this year can be found here: [http://people.tamu.edu/~kevinkrisciunas/ra\\_dec\\_sun\\_2022.html](http://people.tamu.edu/~kevinkrisciunas/ra_dec_sun_2022.html)

Consider making a plot like the top half of Fig. 6, but scale the measured values of the power by the factor given in Eq. 4, with  $k_\lambda = 0.10$  mag/airmass. Fit a line to the data and keep track of the Y-intercept of the plot (and its uncertainty). Do this again for trial extinction values of 0.12, 0.14, 0.16, and 0.18, for example. Then plot those Y-intercepts vs. the trial extinction values and derive the extinction value that would give a Y-intercept of 0.0. In the bottom part of Fig. 6 we see that an extinction term of 0.130 mag/airmass works well for 16 June 2021.

We note that the first point of the day on 16 June was taken when the Sun’s elevation angle was  $3.03^\circ$  (zenith angle  $86.97^\circ$ ) and its airmass (from Eq. 2) was 13.311. With an extinction term of 0.130 mag/airmass, the measured power of 137 Watts implies that the solar panels would have produced 598 Watts (4.37 times as much) if the Sun had been at the zenith and if the solar panels had been tilted to keep angle  $\theta$  the same ( $80.09^\circ$ ).

Alternatively, we could try a range of parameters  $\alpha$  in Eq. 5 to determine the value that gives a regression line of  $P_{extcorr}$  vs.  $\cos(\theta)$  passing through the origin, as we did using  $k_\lambda$  as the extinction term.

In Table 3 we give the derived values of the extinction term  $k_\lambda$  obtained over the past year. The values are plotted in Fig. 7. In spring and summer (26 March to 21 August 2022) our data indicate a median extinction term of 0.145 mag/airmass, with a standard deviation of the distribution of  $\sigma_x = \pm 0.028$ . In fall and winter we find a median extinction term of 0.081 mag/airmass, with a standard deviation of the distribution of  $\sigma_x = \pm 0.020$ . Roughly speaking, the extinction term at our location in the fall and winter is half as large, on average, as in the spring and summer. Table 3 also gives the slopes of the  $P_{extcorr}$  vs.  $\cos(\theta)$  diagrams.

In Fig. 8 we show data obtained on 22 January and 28 May 2022. (The raw data are given in Table 2.) One can clearly see that on these two occasions the power from the solar panels is linearly proportional to  $\cos(\theta)$ , but the proportionality “constant” is not a constant. It depends on the operating temperature of the panels and the transmission of the Earth’s atmosphere.

In Fig. 9 we plot the *slopes* of the  $P_{extcorr}$  vs.  $\cos(\theta)$  diagrams vs. the extinction terms. The data points are color coded and correspond to three ranges of time: January to April, May to August, and October through December.



#### 4. Discussion

In Fig. 10 we plot the atmospheric extinction values obtained by us on 29 nights at CTIO (elevation 2200 m) and LCO (2380 m) from 21 April 2004 through 21 December 2012. The filters used were Johnson  $U, B, V$ , Cousins  $R$  and  $I$ , and the somewhat narrower filters Sloan  $u, r$ , and  $i$ . The median extinction values were 0.510 mag/airmass for  $U$  or  $u$ , 0.267 for  $B$ , 0.154 for  $V$ , 0.113 for  $R$  or  $r$ , and 0.065 for  $I$  or  $i$ . Table 4 of Krisciunas et al. (2017) gives mean extinctions derived from observations of 2004 to 2009 with the 1-m Swope telescope at Las Campanas as part of the Carnegie Supernova Project (CSP-I). We found mean extinction values of  $k_u = 0.511$ ,  $k_B = 0.242$ ,  $k_V = 0.144$ ,  $k_r = 0.103$ , and  $k_i = 0.059$  mag/airmass.

For comparison we consider values of the  $V$ -band extinction measured essentially at sea level. At the nearby Texas A&M Physics Observatory during the colder months the  $V$ -band extinction values range from 0.2 to 0.3 mag/airmass (Carona 2021, private communication). From nine nights of observations near Los Gatos, California (elevation 80 m), from October 1981 to March 1982 we measured mean  $V$ -band extinction of  $k_v = 0.341 \pm 0.050$  mag/airmass. At 75 m elevation near Keaau, Hawaii, on 19 December 1989 (UT) we measured  $k_v = 0.341 \pm 0.020$  mag/airmass on a night that was affected by some volcanic haze. On the next night (clear, but with strong scintillation) we measured  $k_v = 0.187 \pm 0.046$  mag/airmass (Krisciunas 1990).

Let us assert that a sensible estimate of the mean  $V$ -band extinction at sea level under clear sky conditions is  $0.30 \pm 0.06$  mag/airmass. At CTIO and LCO the median or mean extinction is  $0.15 \pm 0.01$  mag/airmass. Thus, the  $V$ -band extinction at sea level is 2.0 times that at CTIO and LCO. By interpolating the data in Fig. 10 we estimate that at a wavelength of 0.76 microns (the middle of the range of wavelengths of light usable by the solar panels) the average atmospheric extinction at the elevations of Las Campanas and Cerro Tololo is about 0.075 mag/airmass. At sea level the extinction at 0.76 microns would then be about  $2.0 \times 0.075 \approx 0.15$  mag/airmass. This may be compared with the median extinction value of 0.145 mag/airmass from data obtained from mid-March through August given in Table 3 and shown in Fig. 7. Recall that the median extinction term derived from solar panel data taken in October through mid-March was 0.081 mag/airmass.

Finally, we consider the efficiency of the solar panels as a function of operating temperature. According to the technical specifications of our panels, the normal operating temperature is  $43 \pm 3$  deg C (109 deg F). The temperature coefficient  $\gamma$  is  $-0.36$  percent/deg K. This means that for every degree the panels are hotter than the normal operating temperature, their efficiency decreases by 0.36 percent.

In Fig. 11 we see an example of how this plays out. The Sun rises and gets higher in the sky. The power corrected to Sun at the zenith increases linearly proportional to  $\cos(\theta)$  until the minimum angle  $\theta$  occurs, then the power begins to decrease. On that particular day between 13:28 and 14:00 CDT the panels began to underperform the regression line fit to data obtained earlier, by about ten percent.

The technical specifications from the manufacturer of our solar panels indicate that the efficiency of the panels will degrade over their 25 year lifetime: “At least 98 percent of nominal power during the first year. Thereafter maximum 0.54 percent degradation per year. At least 93.1 percent of nominal power up to 10 years. At least 85 percent of nominal power up to 25 years.” The analytical method and examples given here would allow the owner of a system of solar panels to evaluate their performance now and in the future.

We thank Don Carona, Nick Suntzeff, and Peter Nugent for useful discussions. We also thank Steven Boada for Python programming advice.

## REFERENCES

- Hardie, R. H. 1962, in *Stars and Stellar Systems, 2, Astronomical Techniques*, ed. W. A. Hiltner (Chicago: Univ. of Chicago Press), 178.
- Herrmann, D. B. 1984, *The History of Astronomy from Herschel to Hertzsprung*, transl. K. Krisciunas (Cambridge: Cambridge Univ. Press)
- Krisciunas, K. 1990, *PASP*, 102, 1052
- Krisciunas, K., Contreras, C., Burns, C. R., et al. 2017, *AJ*, 154, 211
- Landolt, A. U. 1992, *AJ*, 104, 372
- Landolt, A. U. 2007, *AJ*, 133, 2502
- Van Flandern, T. C. & Pulkkinen, K. F. 1979, *ApJS*, 41, 391

Table 1. Raw Data - Part I<sup>a</sup>

Date	CDT	$P_{meas}$	$AZ_{\odot}$	$EL_{\odot}$	$X_{\odot}$	$\theta$
9 Jun 2021	16:07	1779	268.19	53.13	1.2499	53.13
	17:10	863	275.76	39.55	1.5703	68.28
10 Jun 2021	12:31	3859	118.62	75.78	1.0316	9.07
	13:38	3545	201.83	81.95	1.0099	19.96
	14:51	3266	253.24	69.82	1.0654	36.25
	16:16	1322	269.47	51.26	1.2820	55.80
	17:10	680	275.83	39.63	1.5679	68.21
13 Jun 2021 <sup>b</sup>	8:19	1579	75.36	22.35	2.6153	58.24
	9:20	2459	81.73	35.25	1.7327	44.19
	10:06	2885	86.77	45.12	1.4112	33.66
	10:55	3278	93.01	55.70	1.2106	22.71
	11:48	3744	102.65	67.03	1.0862	12.22
	12:24	3909	114.29	74.41	1.0382	8.96
	13:30	3905	187.75	82.61	1.0084	18.21
14 Jun 2021	7:23	513	69.22	10.82	5.2009	71.11
	7:44	900	71.55	15.09	3.7950	66.31
	8:04	1240	73.70	19.21	3.0172	61.73
	8:24	1539	75.81	23.37	2.5086	57.14
	8:41	1812	77.59	26.94	2.1993	53.22
	9:05	2131	80.08	32.02	1.8858	47.70
	9:48	2595	84.66	41.22	1.5176	37.82
	10:10	2801	87.14	45.96	1.3912	32.81
	11:03	3187	94.07	57.39	1.1872	21.05
15 Jun 2021	16:46	822	273.37	45.11	1.4114	62.45
	17:18	586	276.91	38.23	1.6158	69.78
	17:53	363	280.59	30.77	1.9547	77.73
16 Jun 2021	6:45	137	64.53	3.03	13.311	80.09
	7:06	402	67.04	7.17	7.7826	75.34
	7:32	840	70.01	12.39	4.5764	69.42
	7:52	1181	72.20	16.47	3.4907	64.85
	8:03	1375	73.38	18.74	3.0883	62.33
	8:31	1823	76.32	24.57	2.3943	55.90
	9:08	2225	80.16	32.39	1.8668	47.38
	10:03	2923	86.08	44.17	1.4352	34.78
	10:30	3152	89.27	49.99	1.3056	28.68
	11:18	3412	96.10	60.33	1.1508	18.25
	11:54	3531	103.43	67.59	1.0786	11.73
	12:28	3584	114.98	74.94	1.0356	8.99
	13:03	3827	141.54	80.98	1.0125	12.68
17 Jun 2021	8:17	1580	74.91	21.82	2.6753	58.88
	9:13	2330	80.74	33.63	1.8057	46.00
	12:24	3554	113.44	74.31	1.0387	9.10
	14:03	3569	130.77	79.15	1.0182	25.15
	18 Jun 2021	12:00	3641	105.04	69.39	1.0684
	12:58	3711	136.40	80.39	1.0142	12.15
	13:56	3747	224.12	80.32	1.0145	23.57

Table 1—Continued

Date	CDT	$P_{meas}$	$AZ_{\odot}$	$EL_{\odot}$	$X_{\odot}$	$\theta$
	15:11	3060	259.23	65.71	1.0972	40.46
	15:32	2312	263.29	61.23	1.1409	45.28
19 Jun 2021	7:23	697	68.98	10.67	5.2698	71.34
	7:59	1297	72.93	18.01	3.2067	63.11
	9:06	2264	79.93	32.06	1.8839	47.71
	10:27	3074	88.85	49.44	1.3163	29.24
	11:17	3371	95.88	60.22	1.1522	18.39
	11:46	3518	101.46	66.40	1.0912	12.90
	13:08	3873	148.20	81.70	1.0106	13.79
	14:12	3426	237.29	77.68	1.0236	27.05
	15:15	2720	260.06	64.91	1.1042	41.33
	15:46	1993	265.57	58.27	1.1757	48.45
	16:45	900	273.28	45.55	1.4009	62.01
	17:14	674	276.50	39.31	1.5785	68.65
	17:35	501	278.72	34.82	1.7514	73.43
23 Jun 2021	7:03	324	66.59	6.49	8.2685	76.09
	7:29	744	69.57	11.69	4.8333	70.18
	7:59	1266	72.85	17.82	3.2389	63.32
	8:32	1773	76.33	24.69	2.3838	55.73
	9:06	2237	79.85	31.87	1.8941	47.92
26 Jun 2021	7:03	299	66.59	6.32	8.4534	76.25
	7:25	665	69.13	10.72	5.2457	71.24
	8:23	1684	75.41	22.64	2.5843	57.95
	8:46	2050	77.80	27.47	2.1606	52.66
	9:19	2554	81.24	34.47	1.7668	45.07
	9:44	2944	83.90	39.82	1.5615	39.33
21 Aug 2021	8:01	1002	83.66	12.81	4.4345	64.43
	8:02	1016	83.78	13.02	4.3652	64.19
	8:18	1342	85.74	16.46	3.4931	60.32
	8:40	1739	88.46	21.20	2.7483	55.00
	8:59	2050	90.87	25.30	2.3301	50.40
	9:00	2054	91.00	25.52	2.3119	50.16
	9:20	2325	93.64	29.83	2.0046	45.31
	9:40	2850	96.43	34.13	1.7822	40.45
	11:47	3916	123.06	60.00	1.1547	9.72

<sup>a</sup>Column by column we give the date, the Central Daylight Time in hours and minutes, the measured power (in W) from the solar panels, the Sun’s azimuth and elevation angle in degrees, the Sun’s air mass, and the angle in degrees between the vector perpendicular to the solar panels and the direction toward the Sun.

<sup>b</sup>Something is odd about the data of 13 June. We derive the extinction term using the first four points only.

Table 2. Raw Data - Part II<sup>a</sup>

Date	CST/CDT	$P_{meas}$	$AZ_{\odot}$	$EL_{\odot}$	$X_{\odot}$	$\theta$
30 Oct 2021	8:48	1852	115.10	12.92	4.3990	56.82
	9:18	2356	119.77	18.66	3.1004	50.51
	10:01	2883	127.40	26.40	2.2409	42.10
	10:29	3135	133.17	31.01	1.9410	37.26
	11:00	3301	140.28	35.60	1.7177	32.79
	11:29	3411	147.86	39.28	1.5795	29.81
	12:06	3476	158.82	42.87	1.4698	28.32
	12:31	3469	166.94	44.46	1.4276	28.96
	12:58	3383	176.13	45.32	1.4063	31.05
	13:28	3298	186.50	45.17	1.4099	34.78
	14:00	2889	197.23	43.75	1.4461	39.91
	14:10	2793	200.44	43.05	1.4648	41.70
	14:19	2728	203.25	42.33	1.4850	43.37
	14:20	2719	203.56	42.24	1.4874	43.56
	14:30	2531	206.58	41.33	1.5142	45.47
	14:31	2507	206.88	41.23	1.5172	45.67
	14:40	2457	209.50	40.32	1.5456	47.43
14:50	2346	212.32	39.21	1.5820	49.44	
14:56	2295	213.95	38.50	1.6064	50.67	
15:00	2247	215.03	38.01	1.6239	51.50	
15:10	2067	217.63	36.73	1.6721	53.59	
22 Jan 2022	8:04	1303	118.70	8.02	6.8597	61.20
	8:24	1747	121.63	11.75	4.8115	57.17
	8:44	2141	124.75	15.36	3.7304	53.30
	9:04	2477	128.09	18.84	3.0735	49.60
	9:25	2768	131.87	22.31	2.6201	45.98
	9:45	2989	135.74	25.43	2.3198	42.82
	10:04	3172	139.70	28.19	2.1104	40.16
	10:28	3318	145.11	31.35	1.9222	37.37
	10:53	3432	151.25	34.19	1.7793	35.29
	11:52	3499	167.65	38.69	1.5997	34.50
	12:30	3401	179.15	39.64	1.5676	37.13
	13:02	3262	188.90	39.15	1.5839	40.91
	13:37	2968	199.16	37.31	1.6496	46.26
28 May 2022	7:00	396	68.46	5.96	8.8830	75.93
	7:20	733	70.80	10.01	5.5952	71.32
	7:40	1089	73.07	14.11	4.0448	66.70
	8:00	1451	75.28	18.26	3.1649	62.07
	8:20	1784	77.45	22.46	2.6040	57.41
	8:40	2063	79.61	26.69	2.2185	52.75
	9:00	2334	81.78	30.95	1.9446	48.09
	9:20	2581	83.98	35.23	1.7335	43.43

<sup>a</sup>Column headings are like those in Table 1 except the local time is CDT for 30 October 2021 and 28 May 2022, but CST for 22 January 2022.

Table 3. Derived Calibration Values<sup>a</sup>

Date	Extinction (mag/airmass)	Slope (W)	N
13 Jun 2021	$0.124 \pm 0.058$	$3905 \pm 357$	4
14 Jun 2021	$0.183 \pm 0.049$	$3599 \pm 112$	9
16 Jun 2021	$0.130 \pm 0.021$	$3744 \pm 76$	13
19 Jun 2021	$0.138 \pm 0.068$	$3759 \pm 176$	9
23 Jun 2021	$0.152 \pm 0.014$	$3836 \pm 62$	5
26 Jun 2021	$0.173 \pm 0.017$	$4139 \pm 55$	6
21 Aug 2021	$0.181 \pm 0.044$	$4091 \pm 152$	9
28 Oct 2021	$0.030 \pm 0.017$	$4138 \pm 207$	6
29 Oct 2021	$0.072 \pm 0.008$	$4293 \pm 73$	8
30 Oct 2021	$0.051 \pm 0.008$	$4077 \pm 101$	10
5 Nov 2021	$0.081 \pm 0.008$	$4248 \pm 69$	14
14 Nov 2021	$0.100 \pm 0.013$	$4114 \pm 80$	11
23 Nov 2021	$0.085 \pm 0.009$	$4329 \pm 34$	8
21 Dec 2021	$0.097 \pm 0.009$	$4390 \pm 69$	9
3 Jan 2022	$0.067 \pm 0.007$	$4531 \pm 41$	8
16 Jan 2022	$0.092 \pm 0.008$	$4539 \pm 46$	10
22 Jan 2022	$0.093 \pm 0.013$	$4526 \pm 78$	13
29 Jan 2022	$0.074 \pm 0.007$	$4374 \pm 51$	14
5 Feb 2022	$0.065 \pm 0.008$	$4495 \pm 76$	10
13 Feb 2022	$0.054 \pm 0.011$	$4299 \pm 69$	9
19 Feb 2022	$0.086 \pm 0.011$	$4687 \pm 87$	3
12 Mar 2022	$0.091 \pm 0.004$	$4666 \pm 40$	4
26 Mar 2022	$0.136 \pm 0.019$	$4262 \pm 75$	7
9 Apr 2022	$0.127 \pm 0.012$	$4196 \pm 46$	7
26 May 2022	$0.109 \pm 0.005$	$3838 \pm 18$	8
27 May 2022	$0.154 \pm 0.033$	$3850 \pm 63$	7
28 May 2022	$0.120 \pm 0.018$	$3892 \pm 53$	8

<sup>a</sup>“Slope” is the scaling factor of  $\cos(\theta)$ , giving  $P_{extcorr}$ , the power corrected to Sun at the zenith. Angle  $\theta$  is the angular difference of the direction to the Sun and the vector perpendicular to the panels. N is the number of points used to determine the extinction term and the slope.

Fig. 1.— View of the house from the southeast. There are six solar panels on the upper roof and seven on the lower roof.

Fig. 2.— Measured power (in Watts) from the solar panels as a function of time of day. Color coding: 13 June (magenta); 14 June (blue); 16 June (cyan); 19 June (green); 23 June (orange); 26 June (red); 21 August (brown); 9, 10, 15, 17, and 18 June (grey). The vertical dashed line indicates the time of day in June 2021 when the house begins casting a shadow on some of the panels in the lower set of seven.

Fig. 3.— Measured power (in Watts) from the solar panels (Z-axis) as a function of azimuth of the Sun in degrees (X-axis) and the elevation angle of the Sun in degrees (Y-axis). We have excluded data obtained when there was frost on the solar panels, and have also excluded data obtained when shadows were being cast on some of the panels.

Fig. 4.— The plane parallel atmosphere model. Ground level is represented by the solid horizontal line. The extent of the atmosphere is represented by the dashed line. A star at zenith angle  $z$  is observed through a path length of atmosphere that is approximately equal to  $\sec(z)$  times the path length in the direction of the zenith. This ratio of path lengths is called the “air mass” ( $X$ ).

Fig. 5.— The difference of the color-corrected instrumental  $V$ -band magnitudes of photometric standards *minus* the standardized  $V$ -band magnitudes from Landolt (1992, 2007) versus the air mass value (secant of the zenith angle). The data were taken with the 0.9-m telescope at Cerro Tololo Inter-American Observatory by the author on 26 November 2005 (UT). The yellow triangle represents a very blue star measured at high air mass. As it is a  $5\text{-}\sigma$  outlier, it has been eliminated from the fit.

Fig. 6.— *Top*: The measured power output of the solar panel system (in Watts) on 16 June 2021 as a function of the cosine of the angular distance between the vector perpendicular to the solar panels and the direction toward the Sun. The regression line clearly does not pass through the origin. *Bottom*: Same as top diagram, except the power has been corrected to what would have been measured if the Sun were at the zenith and the panels were tilted to the same values of angle  $\theta$ .

Fig. 7.— Derived values of the extinction term  $k_\lambda$  vs. the day of the year.

Fig. 8.— Power (corrected to Sun at zenith) vs.  $\cos(\theta)$  for 22 January and 28 May 2022.

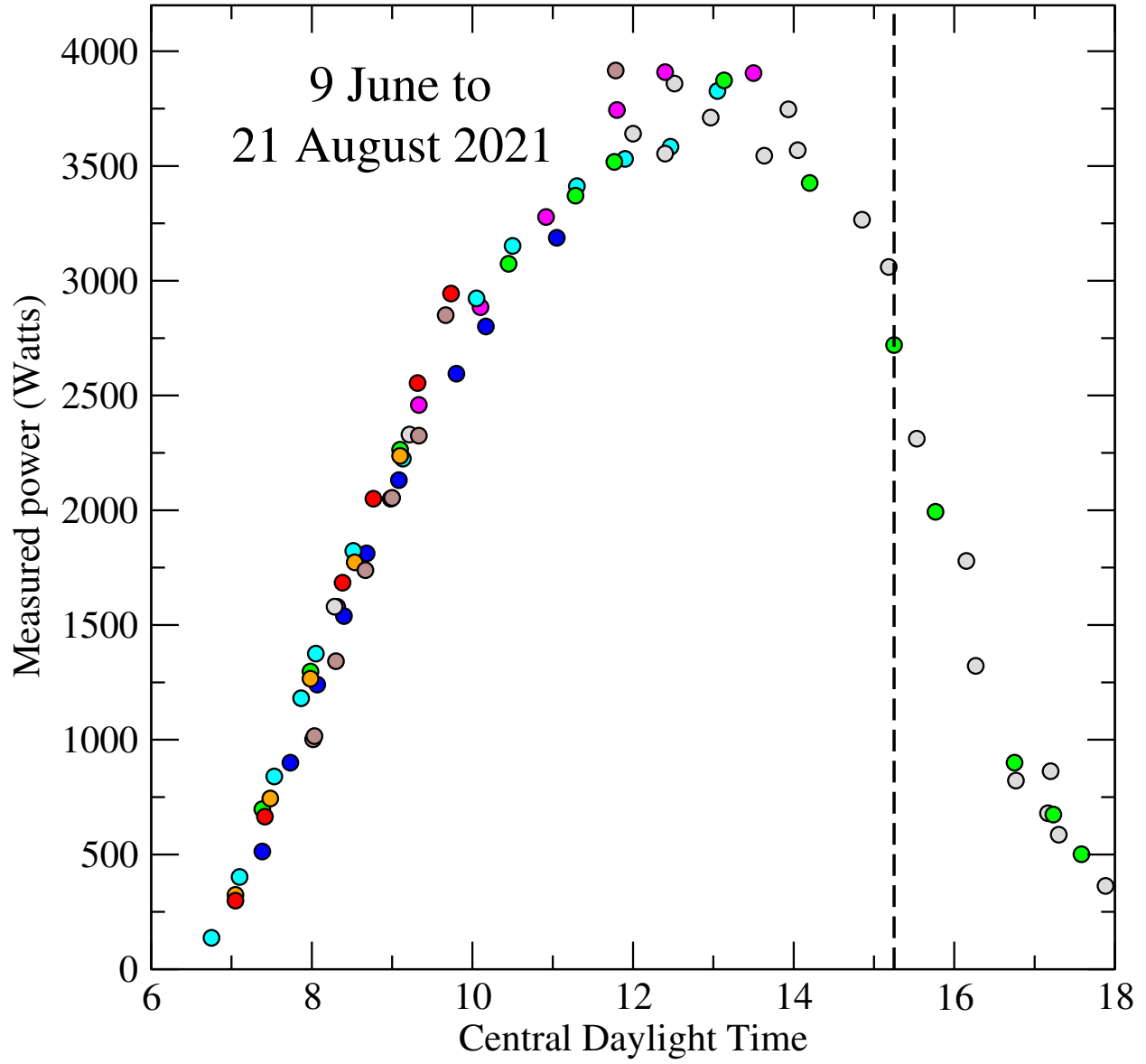
Fig. 9.— Values of the power (corrected to Sun at zenith) vs. the extinction term  $k_\lambda$ . We have color coded the data according to three sets of months.



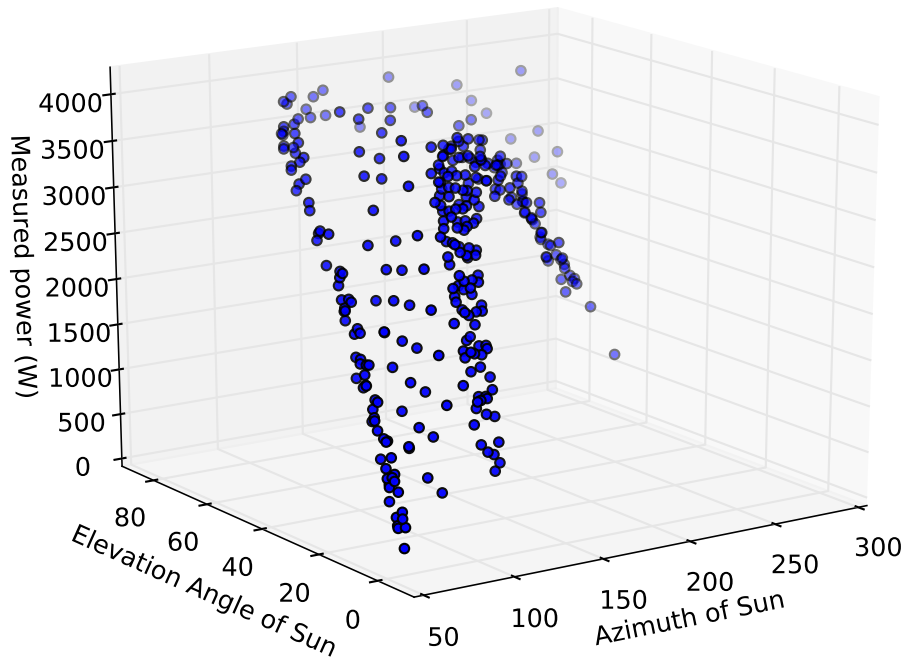
Fig. 10.— The median atmospheric extinction at Cerro Tololo and Las Campanas as a function of wavelength, based on 29 nights of observations by us from 21 April 2001 to 21 December 2012. The filters used were Johnson  $U$ ,  $B$ , and  $V$ , Cousins  $R$  and  $I$ , and Sloan  $u$ ,  $r$ , and  $i$ . The dashed line corresponds to the mean wavelength of functionality of solar panels with silicon-based photovoltaic cells.

Fig. 11.— Power (corrected to Sun at zenith) vs.  $\cos(\theta)$  for 30 October 2021. The raw data are given in Table 2. The solid line is fitted to the blue points. As on many occasions, the solar panels underperform the regression line past a certain time of day. This is most likely due to the decrease in efficiency of the panels when operated at higher temperature. The time stamps are Central Daylight Time.

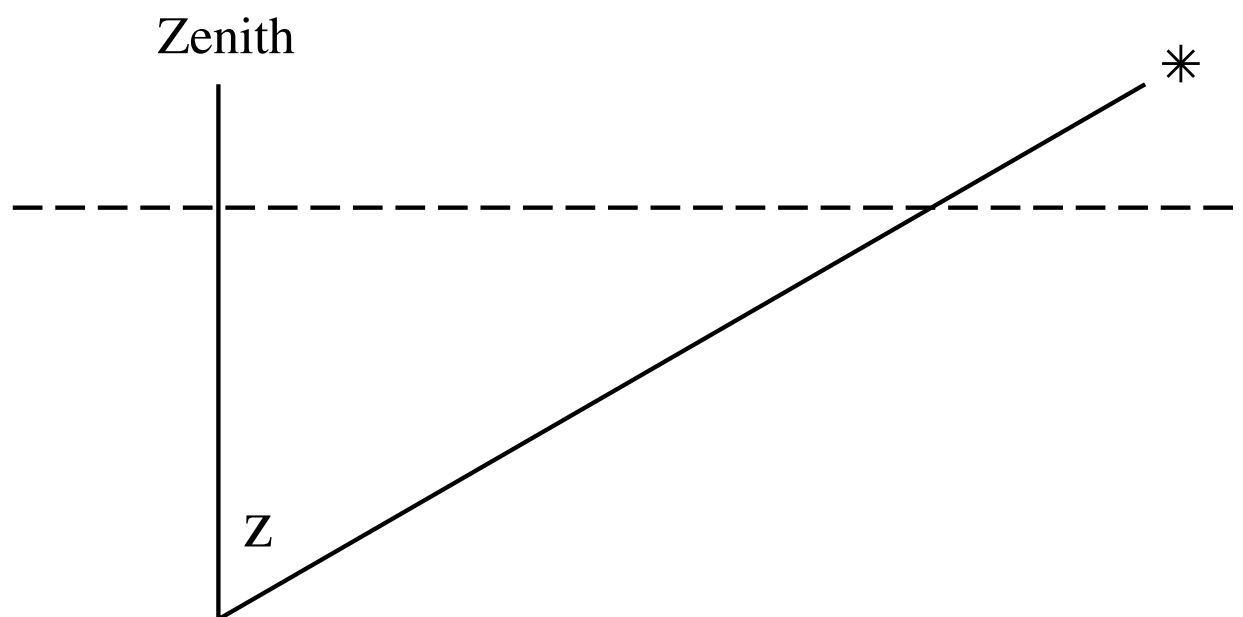




Krisciunas Fig. 2.

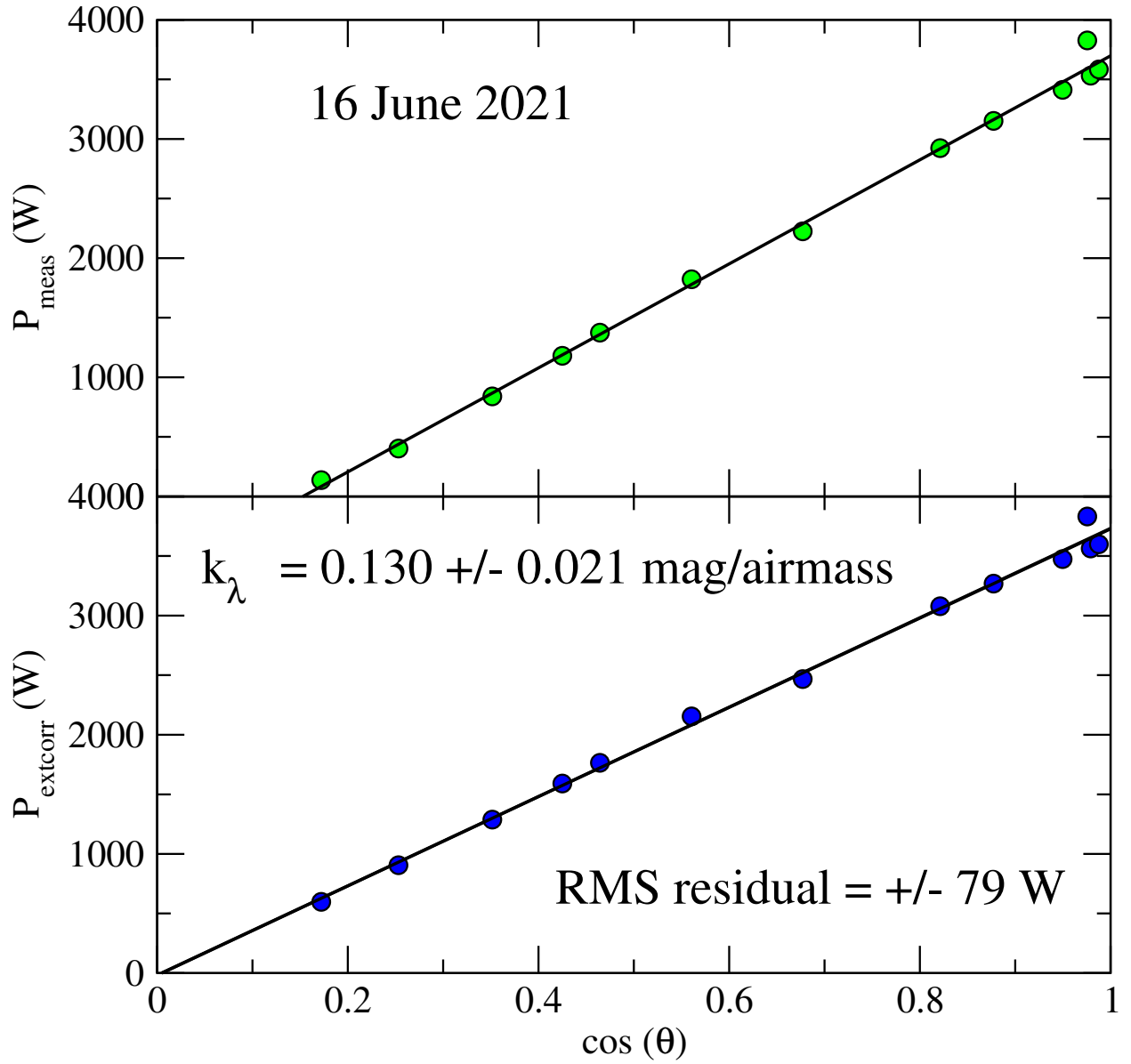


Krisciunas Fig. 3.

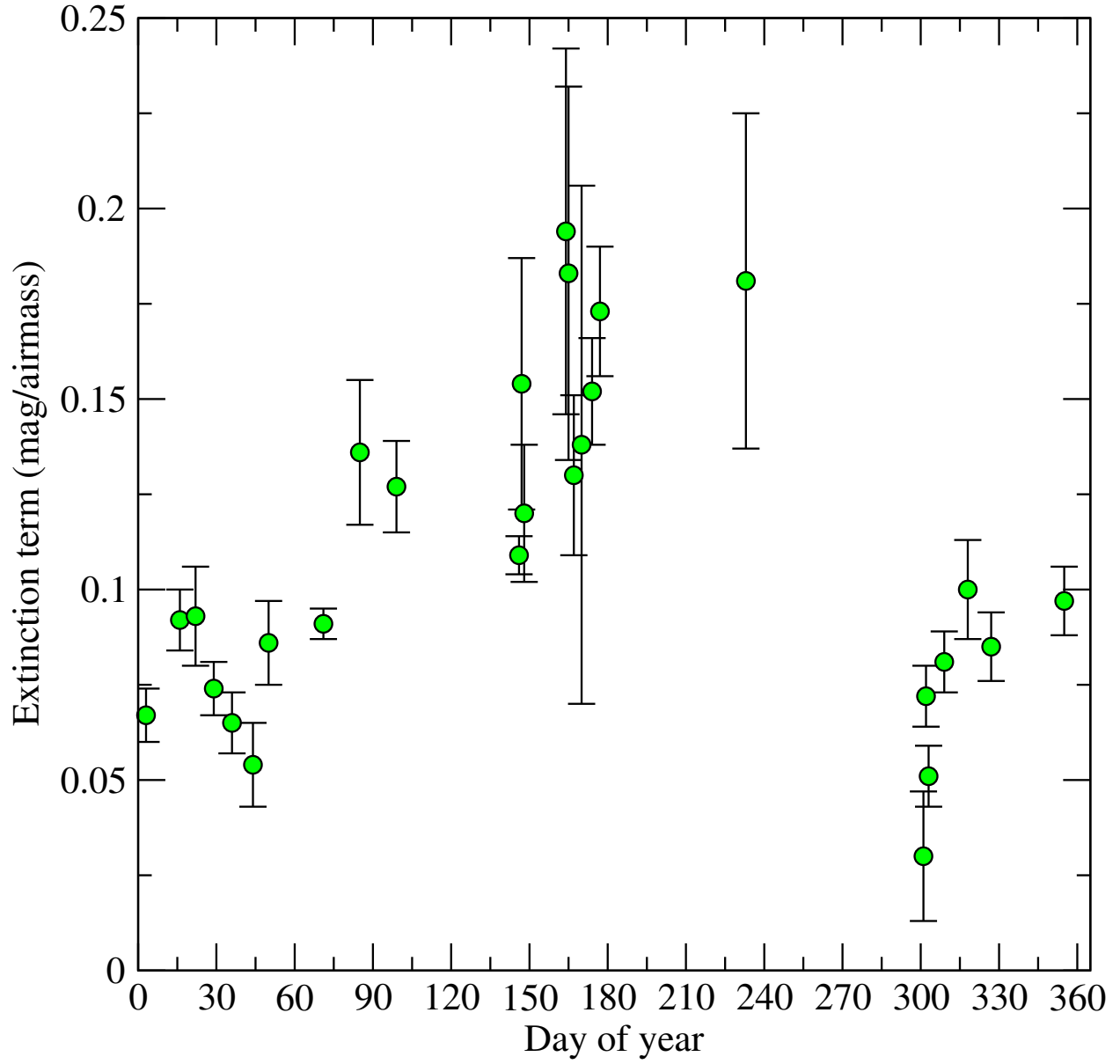


Krisciunas Fig. 4.



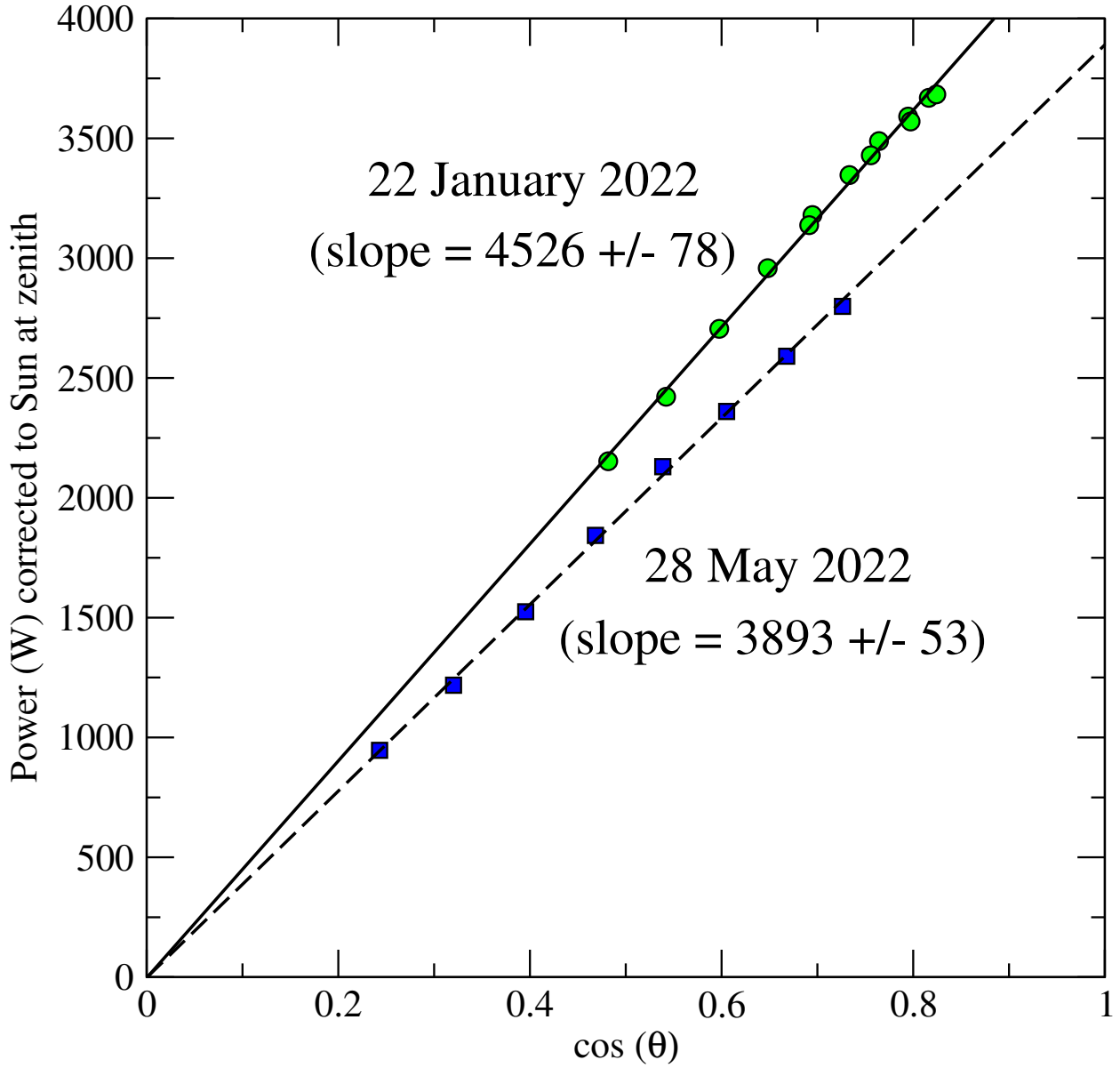


Krisciunas Fig. 6.

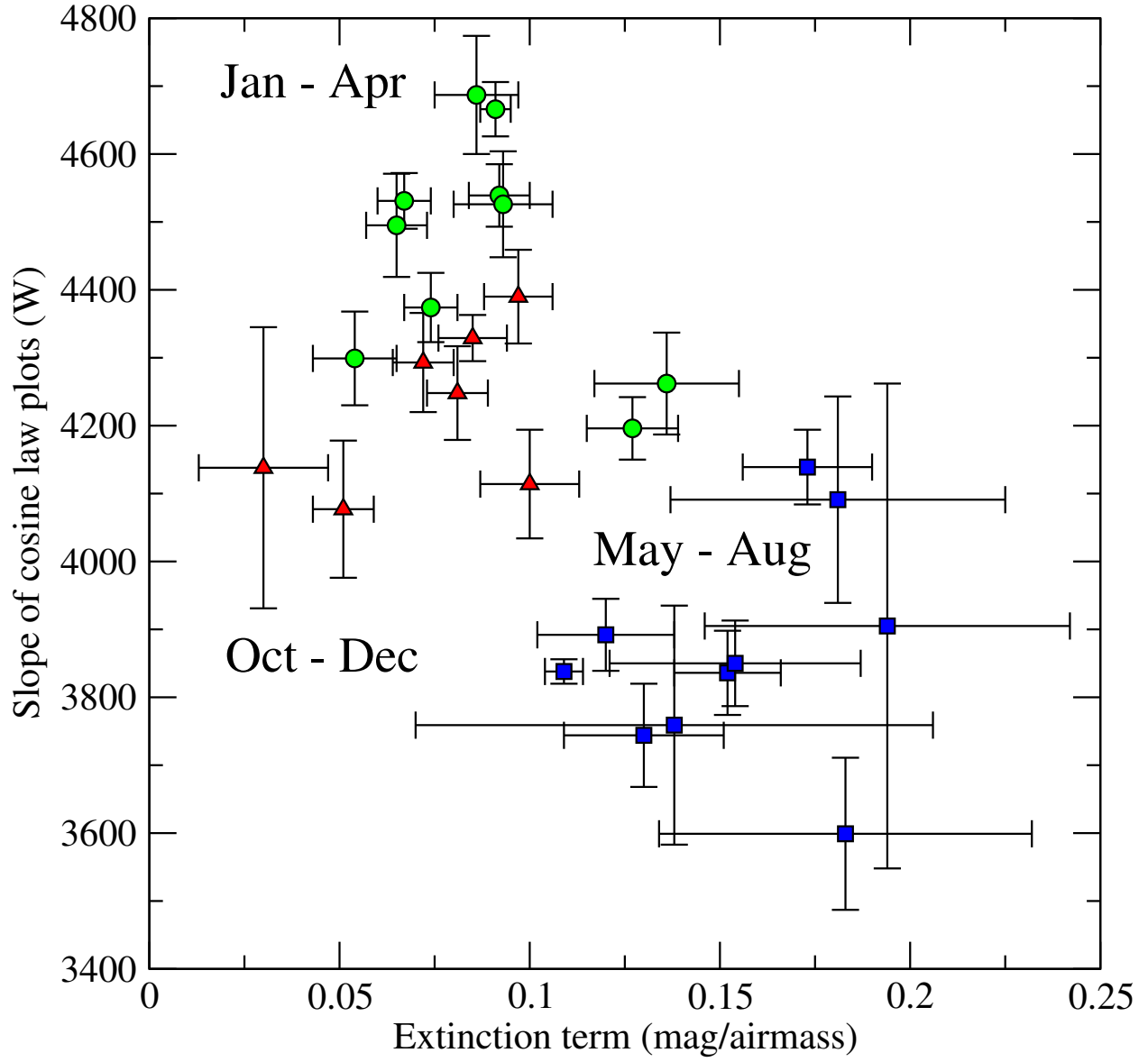


Krisciunas Fig. 7.

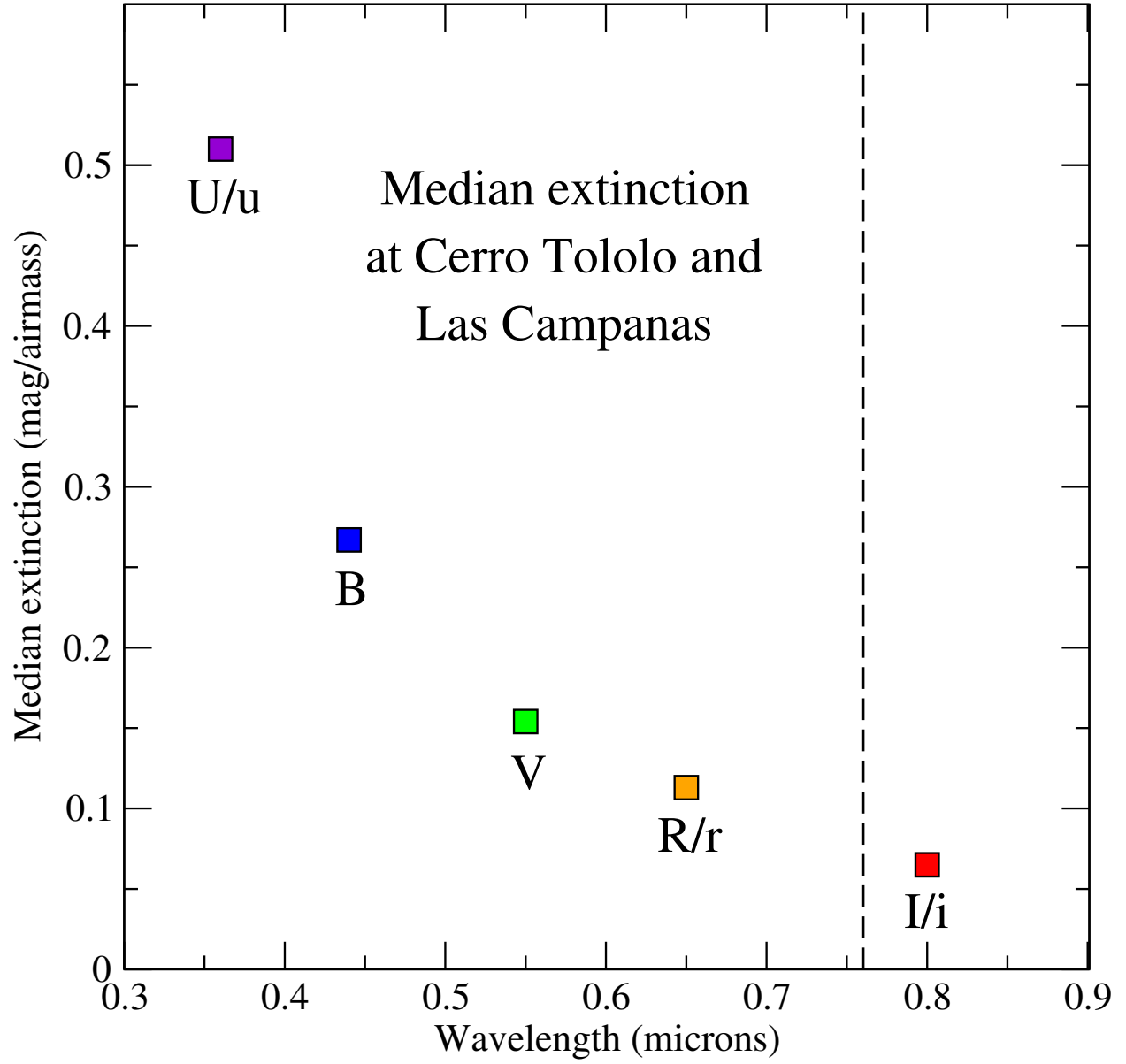




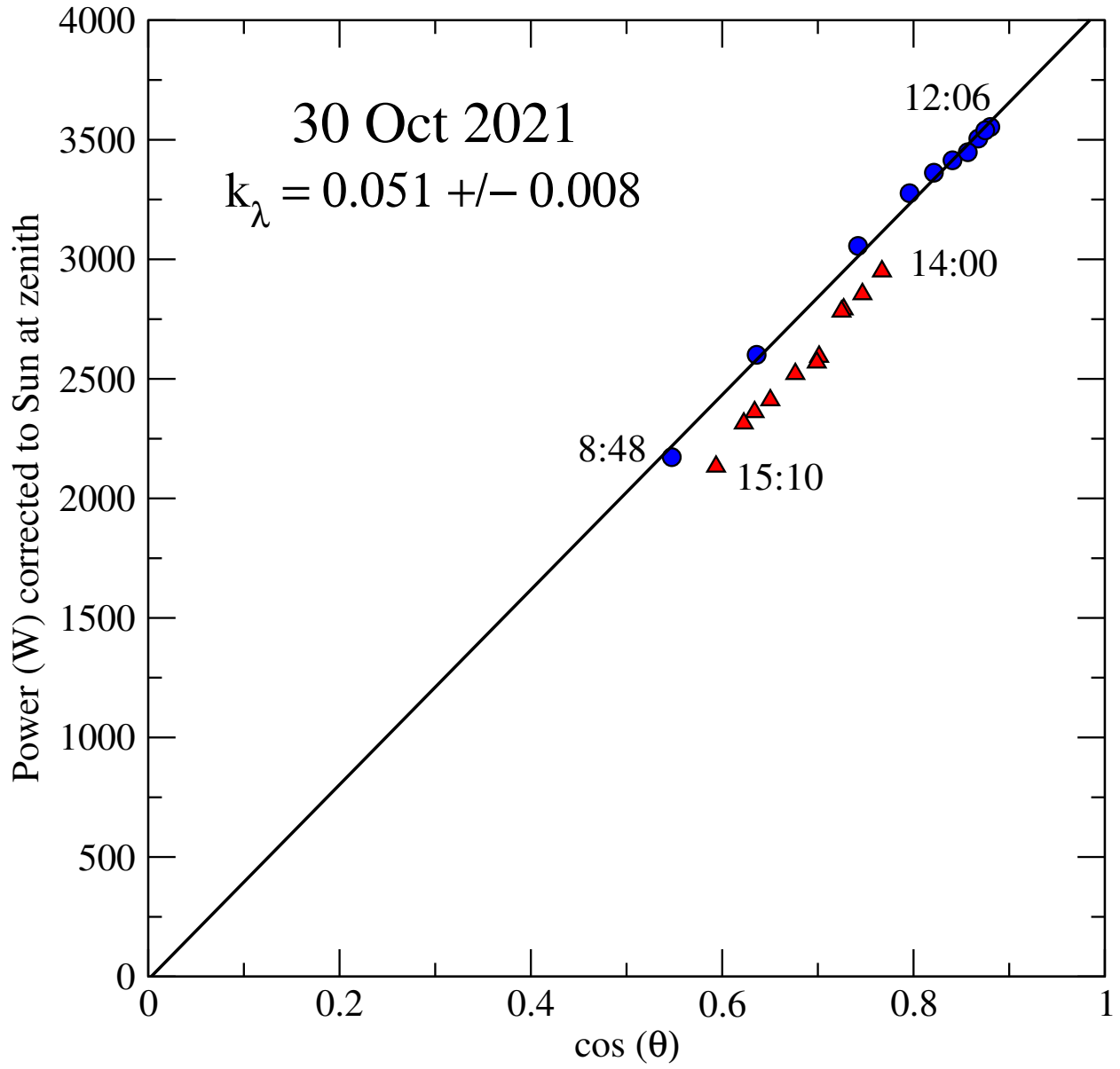
Krisciunas Fig. 8.



Krisciunas Fig. 9.



Krisciunas Fig. 10.



Krisciunas Fig. 11.